Appl. Phys. A (2015) 118:563–568
DOI 10.1007/s00339-014-8757-9

Applied Physics A
Materials Science & Processing

Study on the synthesis and excitation-powerdependent photoluminescence spectrum of ZnSe nanoparticles

Bo Feng · Jian Cao · Jinghai Yang · Donglai Han · Shuo Yang

Received: 8 June 2014 / Accepted: 27 August 2014 / Published online: 7 September 2014

Abstract Zinc selenide (ZnSe) nanoparticles with the cubic zinc blende structure were successfully prepared by a solvothermal method without any surface-active agents. The as-obtained sample was characterized by X-ray diffraction, transmission electron microscopy (TEM), selected area electron diffraction, high-resolution TEM, and room-temperature photoluminescence (PL) techniques. It was proved that EDTA played a significant role during the synthesis of ZnSe nanoparticles. The room-temperature PL spectrum of the ZnSe nanoparticles showed a strong near-band-edge emission peak at 472 nm and a weak defect-related emission band in the range of 600–650 nm. Excitation-powerdependent PL spectrum of the ZnSe nanoparticles showed that the near-band-edge emission peak displayed an evident redshift with increasing the excitation power, and the corresponding energy shift might be as large as 51 meV. In addition, the integrated intensity of the near-band-edge emission peak increased with increasing the excitation power, which indicated the competition between the radiative recombination process and the non-radiative recombination process of photogenerated carriers.

B. Feng (✉) · J. Cao · J. Yang (✉)
Key Laboratory of Functional Materials Physics and Chemistry of the Ministry of Education, Jilin Normal University, Haifeng Street No. 1301, Siping 136000, People's Republic of China
e-mail: fengbosiping@126.com

J. Yang
e-mail: jhyang1@jlnu.edu.cn

J. Yang · D. Han · S. Yang
Key Laboratory of Excited State Physics, Changchun Institute of Optics, Fine Mechanics and Physics, Chinese Academy of Sciences, 3888 Eastern Nan-Hu Road, Changchun 130033, People's Republic of China

1 Introduction

The wide band gap II–VI nanoscale semiconductors have recently attracted substantial attention for optoelectronic applications such as blue lasers, light-emitting diodes, and optical devices [1–3]. By virtue of the wide variation range of the band gap, II–VI semiconductors are suitable for various optoelectronic applications ranging from the far-infrared to the visible and even the ultraviolet spectrum range [4, 5]. Nanoparticles have diverse unique properties including photostability, high fluorescent quantum yield, high resistance to photobleaching, and narrow emission bandwidths, which allow simultaneous excitation of particles of different-sized nanoparticles at a single wavelength [6]. Therefore, the study of nanoparticles has received more attention and drawn considerable interest in both fundamentals and technical application for developing light-emitting devices, lasers, and biological labels [7, 8].

As one of the important Zn-based II–VI semiconductors, due to its wide direct band gap of 2.67 eV, zinc selenide (ZnSe) has been considered to be a promising material for optoelectronic devices, including blue diode lasers, photosensitivity, and photovoltaic solar cells [9–13]. Additionally, ZnSe has significantly large exciton binding energy (21 meV) in comparison with that of GaAs (4.2 meV), which makes it an ideal candidate for efficient room-temperature exciton devices [14, 15]. In recent years, many research groups have developed various strategies to fabricate ZnSe nanocrystals, such as hot-injection methods, reverse micelles methods, and spray pyrolysis [16–18]. Nevertheless, most of these synthetic routes involved expensive organic additives (e.g., tri-*n*-octylphosphine oxide, TOPO), strong reductants (e.g., hydrazine), or toxic SeO_2. For example,

Murase and Gao [17] synthesized blue emitting ZnSe nanocrystals in aqueous solution; however, highly toxic and oxidative H_2Se gas was used as the selenium precursor source. Recently, Xiong et al. [18] reported synthesis of spherical cubic structure ZnSe nanoparticles, but the reaction required a longer time and the selenium precursor used was unstable at room temperature. Therefore, in order to develop technologies that can be used to improve or protect the environment, it is desirable to design and use greener methods to synthesize ZnSe nanomaterials. The solvothermal method is a very effective method for the preparation of inorganic nanomaterials and is confirmed to be an easy-controlled method to synthesize a variety of functional materials with high purity and narrow size distribution [19]. Although the optical properties of ZnSe nanocrystals have been investigated for more than one decade, it is still an interesting work to develop new approaches to the ZnSe nanocrystals with modified optical properties. For example, Jorkaala and Stennenen [20] observed the optical nonlinearity of ZnSe nanocrystals incorporated within polyvinyl alcohol photopolymer matrices by using a pulse nitrogen laser (387.8 nm) as the source of the photoinducing beam. The luminescence properties and transition process of ZnSe are essential for its application in ZnSe-based optoelectronic devices. How to adjust near-band-edge (NBE) emission location and intensity also plays a significant role in the optoelectronic application of ZnSe nanostructures. Until now, although the NBE emission location and intensity can be well adjusted through changing the particle size of ZnSe nanostructures into quantum scope, it is relatively difficult to control the size exactly. A literature search has shown that there is no previous work about the excitation-powerdependent photoluminescence (PL) properties of ZnSe nanoparticles. Such ZnSe materials may be useful for optoelectronic and nonlinear optical applications.

In this paper, we synthesize the ZnSe nanoparticles successfully under mild solvothermal conditions and discuss the growth mechanism in detail. The reaction medium is aqueous solution without any organic solvents or reductants involved. The aqueous synthesis of ZnSe nanoparticles has some advantages such as the moderate reaction temperature, low-toxicity chemicals, and water-soluble products. The room temperature and the excitation-powerdependent PL properties of the ZnSe nanoparticles are investigated. The results indicate that by increasing the excitation power, the NBE emission peak exhibits an obvious redshift. The easy method via adjusting an external light beam to manipulate the PL characteristics should pave an insight for further research on adjustable optoelectronic devices and can also be extended to the study of other nanoscaled semiconductors.

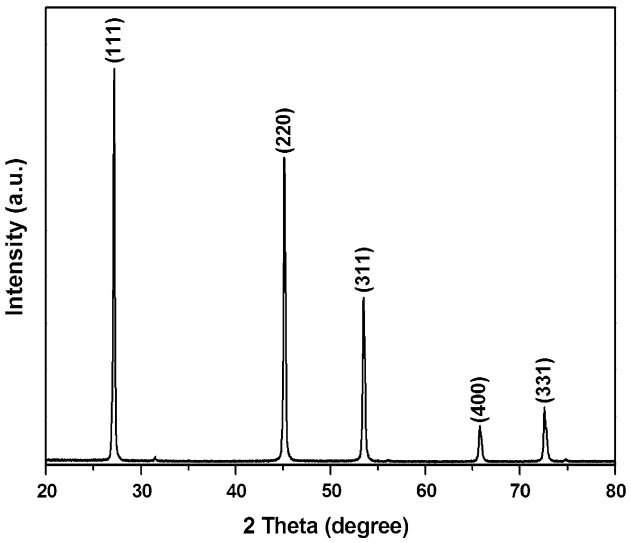

Fig. 1 XRD patterns of ZnSe nanoparticles

2 Experimental

2.1 Preparation of ZnSe samples

All chemicals were of analytical grade and used as received without further purification. The synthesis of ZnSe precursor was carried out by the following procedures: $Zn(NO_3)_2{\cdot}6H_2O$ (0.5 mmol) was dissolved in 30 ml of EDTA solution and selenium powder (99.95 %) (0.5 mmol) in 30 ml NaOH solution. After stirring for 1 h, EDTA solution and NaOH solution were added into one beaker. Then, after stirring for a further hour, the mixed solution was transferred into the 80-ml Teflon-lined autoclave. The autoclave was sealed and heated at 180 °C for 30 h. When the reaction was complete, the autoclaves were cooled to the room temperature. The products were washed with ethanol and deionized water several times, and then separated by centrifugation. They were then dried at 60 °C for 1 h to obtain the precursors. Finally, the precursors were annealed at 300 °C for 2 h to produce the samples.

2.2 Characterization

The crystal structure of the sample was determined using X-ray diffraction (XRD, MAC Science, MXP18, Japan) and high-resolution transmission electron microscope (HRTEM, JEOL JEM-2010). Room-temperature PL spectrum was recorded on a Renishaw inVia spectrometer with a He–Cd laser at the excitation wavelength of 325 nm. The sample was mounted on a xyz-table, which moves the sample to the intersection point of the laser beam and the optical axis to achieve better signal-to-noise ratio. The signals were collected with Olympus camera lens. Multiple curves were recorded to ensure the data reproducibility.

3 Results and discussion

The XRD patterns of the sample obtained by using EDTA and NaOH are shown in Fig. 1. The peaks are assigned to diffraction from (111), (220), (311), (400) and (331) planes of the cubic zinc blende phase of ZnSe, respectively, which are in complete agreement with the PDF card ($F\bar{4}3m$, JCPDS file #37-1463). The lattice constant 'a' for the cubic structure can be determined from the relation:

$$\text{Cubic: } 1/d_{hkl}^2 = (h^2 + k^2 + l^2)/a^2$$

The average lattice constant of 'a' is found to be 5.673 Å, which is slightly larger than the standard value of 5.668 Å. This result indicates that the ZnSe nanoparticles are under tensile strain. Moreover, no diffraction peaks from Zn or other impurities are observed within the detection limit.

Figure 2a shows the TEM images of the sample, indicating the nanoparticles are formed with a spherical shape. The synthesized particle size has a certain distribution. The particle size is in the range of 18.0–24.0 nm. The corresponding particle size distribution is shown in Fig. 2b. The average particle size is about 22 nm. Figure 2c, d represents the HRTEM micrographs of ZnSe, evidencing the highly crystalline nature of the sample. The image clearly reveals the lattice fringes with the distance between two lattice fringes of about 0.33 nm, corresponding to the ZnSe (111) fringe, which is consistent with that of a bulk zinc blende ZnSe crystal. The selected area electron diffraction (SAED) pattern is shown in Fig. 2e. As expected, in the case of nanocrystals, the electron diffraction pattern shows a ring instead of spots due to the random orientations of the nanocrystallites, corresponding to the diffraction from the atomic plane of the nanocrystallites. It presents the selected area diffraction pattern with (220) diffraction plane of ZnSe cubic structure. No patterns for defects or other lattices were observed.

EDTA plays a significant role in the formation of the ZnSe nanoparticles. EDTA in water can be expressed as $[(OOCCH_2)_2NHCH_2CH_2NH(CH_2COO)_2]^{4-}$ and acts as a bridge-like complexing agent, which can combine with Zn

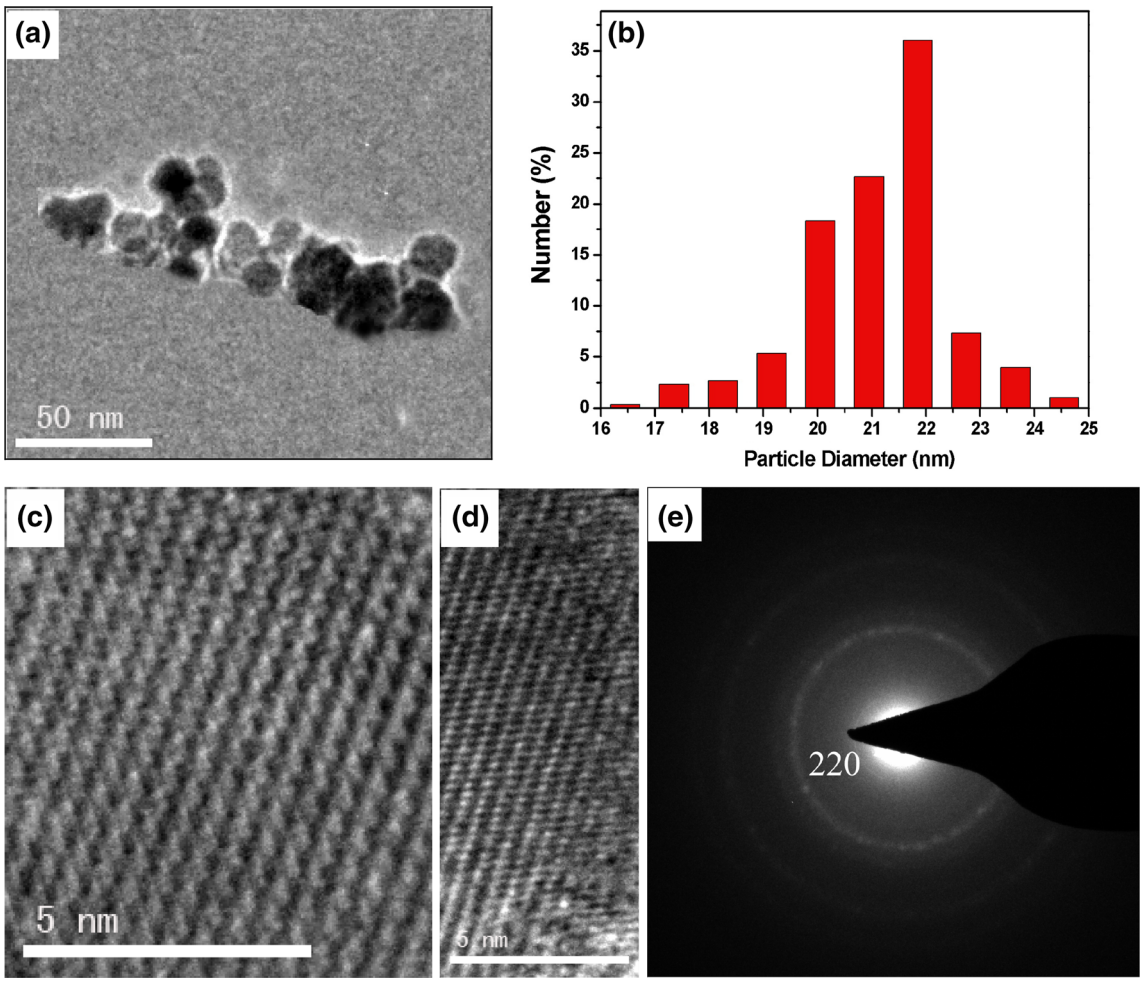

Fig. 2 TEM images (**a**), particle size distributions (**b**), HRTEM image (**c**, **d**) and the corresponding SAED pattern (**e**) of ZnSe nanoparticles

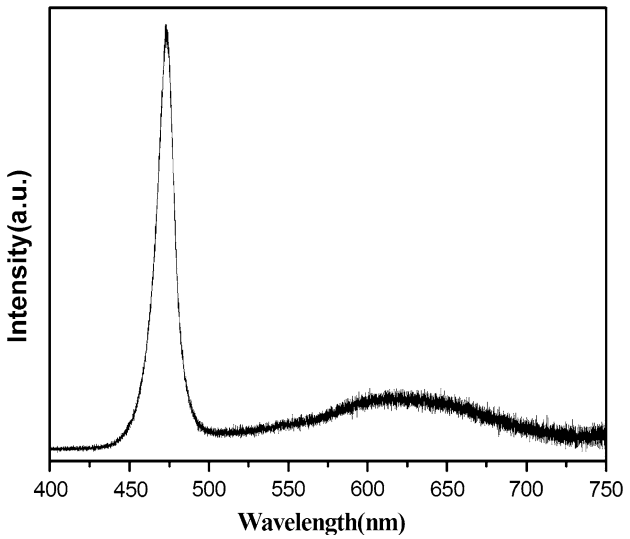

Fig. 3 Room-temperature PL (excited at 325 nm) spectrum of ZnSe nanoparticles

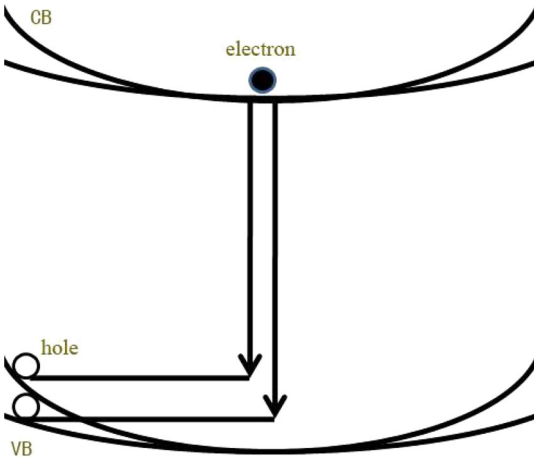

Fig. 4 Schematic illustration of the upward band bending near the surface

ions to form polynuclear complexes by using both ends of the hydrophilic carboxyl group. Then, the chemical reaction between Se ions and Zn^{2+}(EDTA) complexes happens and gradually grows into the primary ZnSe nanoparticles [21]. The standardized NaOH provides a good alkaline environment, adjusting the pH value of the reaction solution. OH^- not only ensures that the Se^{2-} is not oxidized into Se element, but also does not produce $Zn(OH)_2$ precipitate [22]. The mainly reactions in the growth process are shown as follows:

$$3Se + 6OH^- \rightarrow 2Se^{2-} + SeO_3^{2-} + 3H_2O$$

$$Zn(NO_3)_2 + EDTA \rightarrow Zn^{2+}(EDTA) + 2NO_3^-$$

$$Zn^{2+} + 2OH^- \rightarrow Zn(OH)_2$$

$$Zn(OH)_2 + 2OH^- \rightarrow \left[Zn(OH)_2\right]^{2-}$$

$$\left[Zn(OH)_2\right]^{2-} + Se^{2-} \rightarrow ZnSe + 4OH^-$$

$$Zn^{2+}(EDTA) + Se^{2-} \rightarrow ZnSe$$

The room-temperature PL spectrum of as-synthesized ZnSe nanoparticles is shown in Fig. 3. The spectrum shows a strong emission peak at 472 nm that is the NBE emission peak of the ZnSe nanoparticles, arising from the recombination of free excitons through an exciton–exciton collision process [23]. The NBE emission peak of the ZnSe nanoparticles can be estimated to be shifted toward lower energy, when compared to the 2.67 eV (corresponding to 465 nm) band gap of the bulk ZnSe material. ZnSe nanoparticles exhibit intrinsic high surface-to-volume ratio, and from the PL analysis, they possess substantial vacancies, which give rise to the possibility that the electron can be trapped, thereby creating a surface built-in electric field. Synchronously, the vacancies extract electrons from the conduction band of ZnSe and form a depletion layer on the surface, which results in an upward band bending near the surface. Consequently, the upward band bending will reduce the band-gap energy [24]. The schematic illustration of an upward band bending near the surface is shown in Fig. 4. And a defect-related emission band has a weak feature in the range of 600–650 nm [25]. Because the particles are larger than the Bohr exciton diameter of 9 nm in the bulk ZnSe, no quantum size effects has been observed and the optical behavior of the ZnSe nanoparticles is similar to that of the bulk.

Figure 5 shows the room-temperature excitation-powerdependent PL spectrum of the ZnSe nanoparticles. With the excitation power increasing, the NBE emission peak turns sharp and its intensity increases rapidly, indicating the competition between the radiative recombination process and the nonradiative recombination process of photogenerated carriers, consistent with previous report [26]. Moreover, the NBE emission peak displays an evident redshift, and the inset of Fig. 5 shows that the decrease in the peak energy can be as large as 51 meV. The plot of the integrated intensity of the PL peak as a function of the excitation laser power is shown in Fig. 6, and the plot of the integrated intensity of the PL peak as a function of the excitation laser power on a log–log scale is shown in Fig. 7. It can be concluded that the relation is linear. As shown in Fig. 5, the PL spectrum of ZnSe nanoparticles is characterized by the overwhelming exciton recombination peak near the band edge. Therefore, exciton recombination seems to be the dominant way for radiative recombination processes in ZnSe nanoparticles. The integrated intensity of the exciton recombination peak (PL peak) can be written

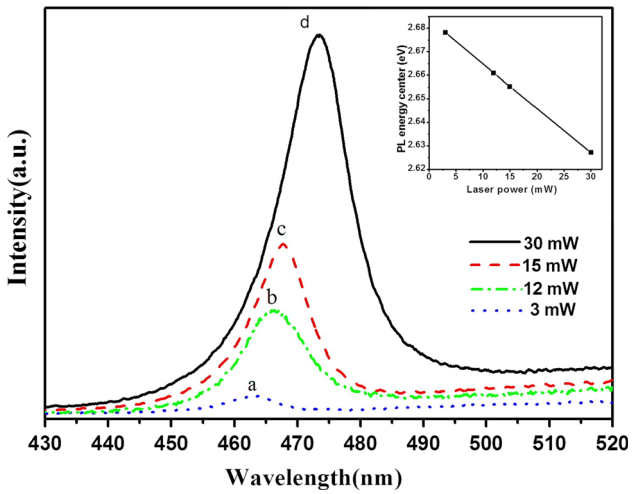

Fig. 5 Excitation-powerdependent of the PL spectra of ZnSe nanoparticles, the inset pattern is the PL peak energy under different excitation power

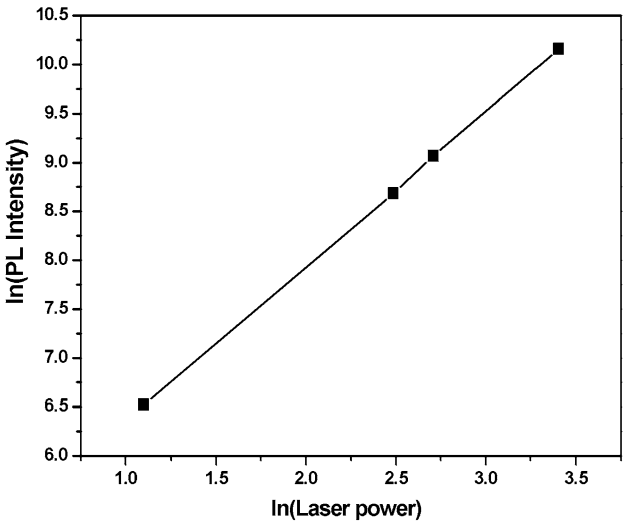

Fig. 7 The *plot* of the integrated intensity of the PL peak as a function of the excitation laser power on a log–log scale

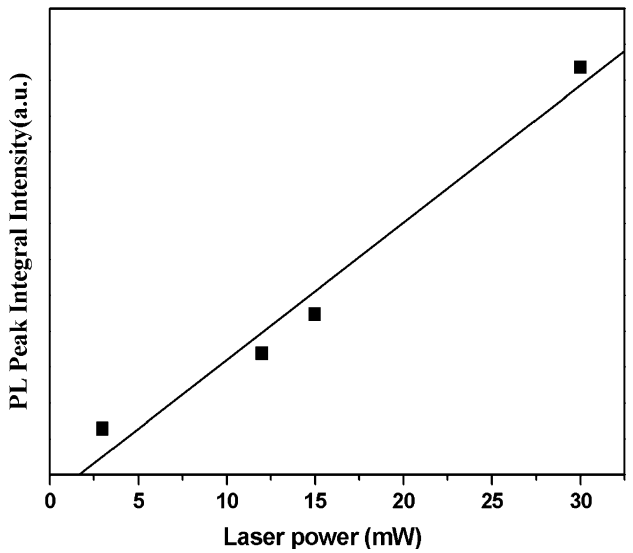

Fig. 6 The *plot* of the integrated intensity of the PL peak as a function of the excitation laser power, and the *solid line* is the best fit to these data

as $I_{PL} \approx np$, where n and p are the population of photogenerated electrons and photogenerated holes, respectively. According to the previous report, if radiative recombination dominates the recombination process of photogenerated carriers, then $P_0 \propto np$ while $I_{PL} \propto np$, so $I_{PL} \propto P_0$, where P_0 is the excitation laser power. When the nonradiative recombination governs the recombination process of photogenerated carriers, then $P_0 \propto n \propto p$ while $I_{PL} \propto np$, so $I_{PL} \propto P_0^2$. Therefore, we can draw the conclusion $I_{PL} \propto P_0^{\alpha}$ [27], where $\alpha = 1$ when radiative recombination dominates the photogenerated carrier recombination process, and $\alpha = 2$ when nonradiative recombination dominates the photogenerated carrier recombination process. So we can infer that when both radiative and nonradiative recombination contribute to the recombination processes of photogenerated carriers, the PL intensity should increase with the excitation power, and α has a value between 1 and 2 [28].

4 Conclusion

In summary, the low-toxic ZnSe nanoparticles have been successfully synthesized by an easy-controlled method. The growth mechanism of as-synthesized ZnSe nanoparticles has also been proposed. The PL results of ZnSe nanoparticles show that there is an NBE emission peak at 472 nm and a weak defect-related emission band in the range of 600–650 nm. With excitation power increasing, the NBE emission peak moves toward the low-energy region for ZnSe nanoparticles, and the peak energy decreases as large as 51 meV for ZnSe nanoparticles. Moreover, the integrated intensity of the NBE emission peak increases with the increase in excitation power, indicating competition between the radiative recombination process and the nonradiative recombination process of the photogenerated carriers. Based on these investigations, the ZnSe nanoparticles are expected to find wide applications in optoelectronic and emission fields.

Acknowledgments This work was financially supported by the National Natural Science Foundation of China (Grant No. 61178074, 61008051, 61378085), Program for the development of Science and Technology of Jilin province (Item No. 201205078, 201215225).

References

1. B.T. Huy, M.H. Seo, P.T. Phong, J.M. Lim, Y. III Lee, Chem. Eng. J. **236**, 75 (2014)
2. D. Colombara, E.V.C. Robert, A. Crossay, A. Taylor, M. Guennou, M. Arasimowicz, J.C.B. Malaquias, R. Djemour, P.J. Dale, Sol. Energy Mater. Sol. Cells **123**, 220 (2014)
3. W. Shi, J. Shi, S. Yu, P. Liu, Appl. Catal. B **138**, 184 (2013)
4. P. Mushonga, I.L.A. Ouma, A.M. Madiehe, M. Meyer, F.B. Dejene, M.O. Onani, Physica B **439**, 189 (2014)
5. D. Li, Q. Ai, X. Xia, Optik **124**, 5177 (2013)
6. K. Byrappa, S. Ohara, T. Adschiri, Adv. Drug Deliv. Rev. **60**, 299 (2008)
7. X. Wang, J. Zhu, Y. Zhang, J. Jiang, S. Wei, Appl. Phys. A **99**, 651 (2010)
8. Z. Chen, D. Wu, J. Lumin. **132**, 2968 (2012)
9. K. Saikia, P. Deb, E. Kalita, Curr. Appl. Phys. **13**, 925 (2013)
10. G.V. Colibaba, E.P. Goncearenco, D.D. Nedeoglo, N.D. Nedeoglo, Infrared Phys. Technol. **62**, 132 (2014)
11. S. Saib, N. Bouarissa, P. Rodríguez-Hernández, A. Munoz, Opt. Mater. **35**, 2303 (2013)
12. D. Wu, Z. Chen, G. Huang, X. Liu, Sensors Actuators A **205**, 72 (2014)
13. D. Shevchenko, J. Mickevičius, N. Starzhinskiy, I. Zenya, A. Zhukov, G. Tamulaitis, Nucl Instrum Methods Phys Res A **749**, 14 (2014)
14. Q. Li, X. Gong, C. Wang, J. Wang, K. Ip, S. Hark, Adv. Mater. **16**, 1436 (2004)
15. J. Wei, K. Li, J. Chen, J. Zhang, R. Wu, J. Alloys Compd. **531**, 86 (2012)
16. D.J. Kim, K.K. Koo, Cryst. Growth Des. **9**, 1153 (2009)
17. N. Murase, M.Y. Gao, Mater. Lett. **58**, 3898 (2004)
18. S. Xiong, S. Huang, A. Tang, F. Teng, Mater. Lett. **61**, 5091 (2007)
19. S. Jana, I.C. Baek, M.A. Lim, S. Il, Seok. J. Colloid Interface Sci. **322**, 473 (2008)
20. H. Jorkaala, H. Stennenen, J. Opt. A Pure Appl. Opt. **4**, 366 (2002)
21. F. Cao, W.D. Shi, L.J. Zhao, S.Y. Song, J.H. Yang, Y.Q. Lei, H.J. Zhang, J. Phys. Chem. C **112**, 17095 (2008)
22. X. Wang, L. Li, Y. Lin, J.J. Zhu, Ceram. Int. **39**, 5213 (2013)
23. Y. Yang, Y. Zhang, X. Zhou, X. Wu, S. Xu, H. Wu, S. Guo, Nano Biomed. Eng. **3**, 107 (2011)
24. T. Gao, T.H. Wang, Appl. Phys. A **80**, 1451 (2005)
25. H. Wang, T. Tian, S. Yan, N. Huang, Z. Xiao, J. Cryst. Growth **311**, 3787 (2009)
26. F. Wang, Z. Zhang, R. Liu, X. Wang, X. Zhu, A. Pan, B. Zou, Nanotechnology **18**, 305705 (2007)
27. Z. Hung, A. Ioannidis, M.F. Lawrence, J. Phys. Chem. **97**, 952 (1993)
28. S.Z. Wang, S.F. Yoon, L. He, X.C. Shen, J. Appl. Phys. **90**, 2314 (2001)